Title

Large-scale structure of the fast solar wind

Journal

Journal of Geophysical Research-Space Physics, 112

ISSN

0148-0227

Authors

Bisi, M. M.
Fallows, R. A.
Breen, A. R.
et al.

Publication Date

2007-06-01

DOI

10.1029/2006JA012166

Peer reviewed

Large-scale Structure of the Fast Solar Wind

M. M. Bisi,[3] R. A. Fallows,[1] A. R. Breen,[1] S. Rifai Habbal,[2] and R. A. Jones[1]

Abstract. We present the results of a comprehensive study of the fast solar wind near solar minimum conditions using Interplanetary Scintillation (IPS) data taken with the EISCAT system in northern Scandinavia and a recent extremely long baseline observation using both EISCAT and MERLIN systems. The results from IPS observations suggest that the fast wind inside $100\,R_\odot$ can be represented by a two-mode model in some cases but this distinction is much less clear by in-situ distances beyond 1AU. Two distinct fast streams are seen in the extremely long baseline IPS observation; comparison of the IPS line of sight with a synoptic map of white light indicates the faster mode overlies the polar crown and the slower fast mode overlies an equator-ward boundary of the polar coronal hole.

1. Introduction

Interplanetary Scintillation (IPS) is the rapid variation in the signal received by radio antennas at Earth from a compact radio source arising from scattering by small-scale (~100 km) density variations in the solar wind. Measurements of IPS allow the solar wind velocity to be inferred over all heliographic latitudes and a wide range of heliocentric distances [e.g. *Dennison and Hewish*, 1967]. When two radio telescopes are used and the separation of the raypaths in the plane of the sky from source to each telescope is close to the radial direction centered at the Sun, a high degree of correlation between the scintillation patterns recorded at the two telescopes may be observed [e.g. *Armstrong and Coles*, 1972a; *Coles*, 1996]. The time lag for maximum cross-correlation can be used to estimate the outflow speed of the irregularities producing the scintillation. More sophisticated methods involving fitting the results of a scattering model to the observed auto- and cross-spectra may also be adopted [e.g. *Coles et al.*, 1995; *Coles*, 1996; *Klinglesmith*, 1997].

In weak scattering, the observed scintillation pattern can be treated as arising from the sum of all the scattering events along the raypath. If the raypath passes through two or more streams of solar wind, their contributions are independent and can be modelled separately provided that their location along the raypath can be established. Studies using the European Incoherent SCATter (EISCAT) IPS data set have confirmed that the best results of fitting a weak scattering model to the data [*Coles*, 1996; *Klinglesmith*, 1997] are obtained if regions of the raypath overlying dark regions in white light observations are assumed to be immersed in fast wind and slow streams are assumed to overlie high intensity white light regions identified with streamers [*Coles*, 1996]. Throughout these discussions we define "polar crown flow" as the central region of the polar fast streams (as seen in interplanetary space) and "flank flow" as the region of fast flow between this crown outflow and the equator-ward boundary of the fast stream.

Ulysses observations from the first polar pass (1994-1996) revealed the existence of a latitudinal gradient in the fast wind speed across the polar regions, with the highest velocities measured at the highest latitudes [*Phillips et al.*, 1995; *Goldstein et al.*, 1996; *Woch et al.*, 1997; *McComas et al.*, 2000; *Habbal and Woo*, 2001]. The boundary between the fast and slow outflow measured by Ulysses was located at about ± 20° around the heliographic equator [*Woch et al.*, 1997].

[1]Institute of Mathematical and Physical Sciences, University of Wales, Aberystwyth, GB

[2]Institute for Astronomy, University of Hawaii, USA

[3]Center for Astrophysics and Space Sciences, University of California, San Diego, 9500 Gilman Dr., La Jolla, CA 92093

0148-0227/06/$9.00

The most commonly accepted view of the fast wind places its origin within polar coronal holes, at the centre of the supergranular cells [*Dupree et al.*, 1996] or the boundaries of supergranular cells [*Hassler et al.*, 1999]. This view implies a subsequent superradial expansion of the boundaries of the polar outflow so that the fast wind can occupy a significant volume of the heliosphere, as observed by Ulysses at solar minimum. However, using white light, radio ranging and ultraviolet spectroscopic observations in the inner corona, Woo and Habbal (1997) and Habbal and Woo (2001) suggested that the fast wind originates in the quiet Sun as well as in the polar coronal holes, and that the outflow is predominantly radial. In the latter scenario, the fast solar wind from the quiet Sun wind would be expected to be marginally slower and slightly denser than the outflow from the polar coronal hole.

In this paper we use IPS data from EISCAT [*Rishbeth and Williams*, 1985; *Wannberg et al.*, 2002] taken during the last solar minimum (1994 through to 1997) supplemented by in-situ measurements from the Ulysses|SWOOPS (Solar Wind Observations Over the Poles of the Sun) [*Bame et al.*, 1992] instrument, observations from LASCO (Large Angle Spectroscopic COronagraph) [*Brueckner et al.*, 1995] and EIT (Extreme ultra-violet Imaging Telescope) [*Delaboudiniere et al.*, 1995] instruments on SOHO (SOlar and Heliospheric Observatory), as well as images from the Mauna Loa Mk III coronagraph [*Fisher et al.*, 1981], and the Yohkoh [*Ogawara*, 1987; *Ogawara et al.*, 1991]|SXT (Soft X-ray Telescope) [*Acton et al.*, 1989] instrument to investigate whether there is evidence of a two-mode structure within the fast solar wind, as originally proposed by Woo and Habbal (1997). In carrying out this investigation, two main questions were considered: First, is the solar wind best represented by a two-mode fast wind; and second, is the boundary between two modes of fast wind related to the coronal hole boundaries seen in EUV and X-ray. We first describe the data (section 2), and the data analysis tools used to infer flow speeds (section 3). The findings are discussed in section 4, followed by concluding remarks in section 5.

2. Observations

Woo and Habbal [1997] suggested that a small step in density seen in the Ulysses data indicated the presence of two modes of fast wind, with the fastest (and least dense) emerging radially from the polar coronal hole and a second, slightly slower and denser stream emerging from the quiet Sun. An EISCAT observation of 0741+271 above the north polar coronal hole on 1995 July 11 appeared to be better represented not by fast and slow streams but by a two-mode fast wind, prompting a study into this question.

In this study it was deemed important to consider only low-noise, high-latitude data from fast-wind dominated observations of simple, isolated radio sources. Only data from observations at elevation angles of around 10° or more were considered. The scattering model assumes that all the scintillation comes from a single point source in the centre of the beam. Structured or multiple

sources in the beam will give rise to superpositions of scintillation patterns which, at present, cannot be fitted in a manner which is not misleading. The sources used are all primary calibrators at 21cm wavelength for the "A" configuration of the VLA. Thus they have no decorrelation over 35km but they could still have a small effect on the IPS, for which the Fresnel Radius at an observing wavelength of 32cm is approximately 90km.

For the scintillation to be strong enough for the signal spectrum to be clearly resolved but not so strong as to start to come into the strong scattering regime in the fast solar wind, only observations for which the point of closest approach of the raypath to the Sun lay between $15\,R_\odot$ and $120\,R_\odot$ were considered. In the past, this has proven to be the best range when considering mid- to high-latitude fast solar wind observations at this frequency. This eliminates possible distortion of the results by the effects of strong scattering.

In order to detect small variations in the fast solar wind structure, it is necessary to eliminate observations containing a significant amount of slow wind. This was done using a two-stage selection process. In the first stage any observation in which less than 30° of the raypath around the point of closest approach to the Sun lay above the coronal hole was eliminated. This provided a quick way of eliminating observations containing a large proportion of slow solar wind. The list of observations was then refined by calculating the proportion of scintillation being generated in the region of the raypath which overlay the coronal hole. Only observations in which more than 85% of the scintillation came from above the coronal hole were considered for the main study. The slow wind was assumed to scintillate 3.5 times more than the fast wind in this calculation – this is likely to be an overestimate, as EISCAT observations suggest that the density variations in the slow wind are normally 2-3 times greater than those in the fast wind over the distance range considered in this study [*Fallows et al.*, 2002b], thus giving us considerable confidence that we were indeed eliminating observations which contained a significant proportion of slow wind.

The majority of the IPS observations discussed in this paper were made between 1994 and 1997 using the EISCAT radio telescopes. The receiving frequency was on a 10 MHz bandwidth centred on 933.5 MHz from 1994 to 1995 and an 8 MHz bandwidth centred on 931.5 MHz from 1996 to 1997. A single extremely long-baseline observation combining data taken at 1420 MHz by EISCAT and MERLIN telescopes in northern Scandinavia and the UK respectively [*Bisi et al.*, 2005; *Breen et al.*, 2006] is discussed in section 4.3.

The Ulysses data used in this paper are hourly-averaged SWOOPS ions radial velocity data taken during the first polar pass of the Sun. The data were from the mid- to high-latitude southern and northern polar passes where the solar wind velocity did not dip below $600\,km\,s^{-1}$ for each hourly-averaged data-point used, thus eliminating interaction regions and periods of large variations in velocity seen at the slow to fast wind transition in the Ulysses velocity data.

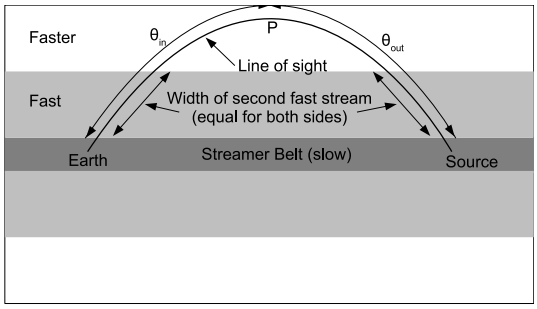

Figure 1. Diagram demonstrating the geometry of the new model including two fast streams. The line of sight is displayed as though it were mapped back down to the corona. It should be noted that, although the second fast stream width is fixed for both sides of the line of sight, each tail end above the streamer belt may have a variable width.

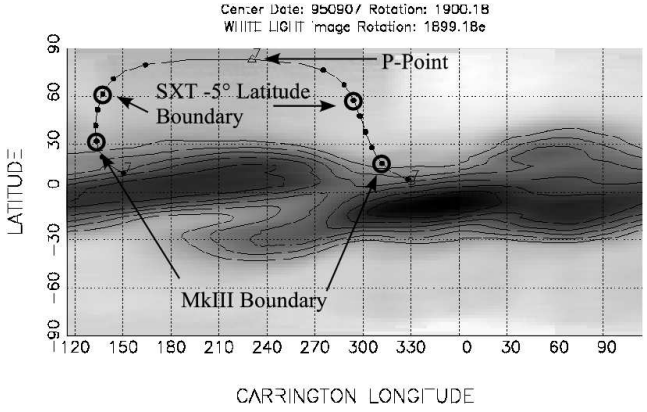

Figure 2. A white light map of the East limb of the Sun, Carrington Rotations 1889-1900 centred on 1995 September 8, constructed using data taken from the Mauna Loa MkIII Coronagraph at $1.7\,R_\odot$ with the IPS raypath mapped onto it and both SXT -5° latitude and MkIII coronal hole boundaries circled as well as the P-Point, the point of closest approach of the IPS raypath to the Sun in the plane of the sky.

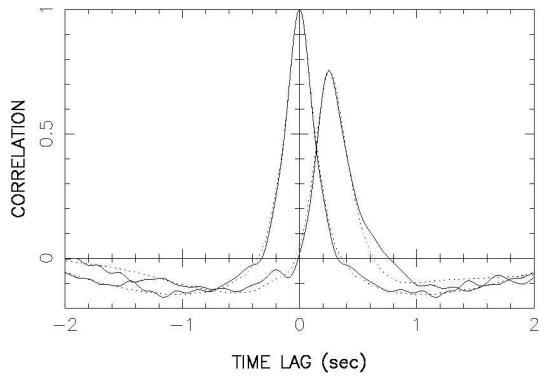

Figure 3. The EISCAT IPS observation of J1120+143 on 1995 September 8, fitted with the two-stream weak scattering model (dotted line). The power law exponent α was set to 3.0, the inner scale to 35km and the axial ratios of the fast and slow streams to 2.2 and 1.5 respectively. The dominant fast stream has a velocity of $883\,km\,s^{-1}$ with a random radial component of $256\,km\,s^{-1}$. The slow stream has a fixed velocity of $350\,km\,s^{-1}$.

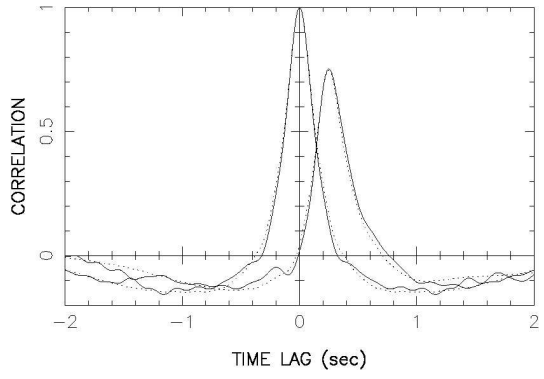

Figure 4. The EISCAT IPS observation of J1120+143 on 1995 September 8, fitted with the three-stream weak scattering model (dotted line). The spectral and slow stream parameters are set as in Figure 3. The faster and fast velocities are $875\,km\,s^{-1}$ and $596\,km\,s^{-1}$ respectively with a fast stream width of 16°.

Table 1. Summary of IPS results

Date	Source	Vfast	dvpar	Vmid	Width(in)	Width(out)	rmsV	Vslow	θ_{in}	θ_{out}	wtslow	AR	α	iscale	χ^2_ν
950714	0741+312	742	459				80	300	-65°	70°	8	1.8	3.0	36	3.17
		855		439	28°	28°									**2.32**
		942		501	35°	40°									3.74
950906	1120+143	809	210				0	450	-70°	60°	3	2.3	3.0	35	5.88
		852		554	18°	18°									**3.55**
		933		765	50°	40°									6.84
950907	1120+143	871	214				0	450	-70°	60°	2	2.0	3.0	35	3.67
		896		703	29°	29°									**2.97**
		939		783	45°	35°									3.85
950908	1120+143	883	256				0	350	-70°	60°	2	2.2	3.0	35	1.88
		875		596	16°	16°									**0.93**
		977		765	50°	35°									1.61
960529	0336+323	834	143				0	350	-75°	75°	8	1.8	3.0	57	1.94
		842		730	25°	25°									1.35
		926		805	65°	45°									1.76
960608	0521+166	804	152				0	350	-65°	80°	8	1.7	3.0	26	6.85
		847		763	40°	40°									6.36
		882		751	55°	30°									6.60
960609	0521+166	773	210				0	350	-70°	80°	4	1.5	3.1	25	3.92
		877		716	49°	49°									**3.24**
		897		732	55°	55°									4.27
960817	0954+177	839	406				0	450	-60°	60°	10	3.5	2.5	8	1.15
		981		660	26°	26°									1.20
		985		627	35°	35°									1.82

3. Data Analysis

A weak scattering interplanetary scintillation model allowing for the presence of two solar wind streams in the line of sight has been used for the last decade to analyse EISCAT IPS observations [e.g. *Coles*, 1996; *Klinglesmith*, 1997; *Canals*, 2002]. The current analysis routines perform all fitting to the auto- and cross-power spectra, with the resulting correlation functions displayed for a more convenient visualisation.

The power spectrum of the density variations in the solar wind giving rise to IPS is described by a power law with exponent α, cut off by an "inner scale" corresponding to the dissipation scale of the turbulence. Previous studies [e.g. *Yamauchi et al.*, 1996] have found α to vary between 2 and 4 and the inner scale in kilometres to be roughly equal to the distance of the observation in solar radii, although it is not very well determined. We adjust these parameters to match the high-frequency tail of the auto- power spectrum. The density variations are assumed to be anisotropic and normally extended in the radial direction. The model assumes that a fast stream will be present in the central portion of the line of sight, flanked by a slow stream at either end. The slow stream is given an extra weighting to account for its greater density and hence greater scattering power. Following the work of *Little and Ekers* [1971], each stream can be modelled as having a mean speed with random velocity components in the radial ($\delta V_\parallel$ - indicated by a skewed cross-correlation function) and transverse ($\delta V_\perp$ - indicated by a reduced area under the cross-correlation function) directions.

This work required the model to be extended to allow for a third stream in the line of sight. This had to be done in such a way that the total number of free parameters was not substantially increased. To achieve this, the velocity of a second fast stream was modelled in place of the $\delta V_\parallel$ of the main fast stream. The second fast stream was assumed to have the same remaining properties ($\delta V_\perp$ and axial ratio) as the main fast stream and to occupy a band above the main streamer belt (Figure 1). The second fast stream was given an additional weighting of 1.5 according to the increase in Ulysses' density values above the quiet Sun noted by *Habbal and Woo* [2001]. This results in a model which can either assume a single fast stream with a random radial component or assume two discrete fast streams with the second occupying a variable band above the streamer belt – an increase of only one free parameter. The model will also allow the width of the second fast stream to be different on each side of the line of sight but this is only for the purpose of fixing the fast/faster stream boundary to the coronal hole boundary seen in EUV and X-ray for a direct comparison. No fit is performed involving both widths independently.

The region of the IPS raypath overlying the polar coronal hole – and hence assumed to be immersed in the fast stream – is estimated by ballistically projecting the raypath down onto a white light map constructed from either Mauna Loa MkIII data or, when available, from SOHO|LASCO observations. Determination of the region of the raypath overlying the X-ray coronal hole is carried out in similar fashion using synoptic maps constructed from Yohkoh|SXT and SOHO|EIT measurements. In the analysis routines the portion of the raypath above the coronal hole is described in terms of two Sun-centred angles along the raypath from the point of closest approach, θ_{in} (Earth side of the line of sight) and θ_{out} (source side of the line of sight). These two angles are illustrated in Figure 1. The assumption of a fast stream flanked by slow flow is normally a valid one since the geometry of the line of sight between Earth and the radio source usually ensures that the tail ends lie above the equatorial streamer belt. Furthermore, since the level of scattering giving rise to IPS falls as $1/R^4$, a fast stream in the tail of the line of sight will not have any effect on the measurements in comparison to the much denser slow stream. However, slow flow in the tails of the line of sight will still have an effect.

Figure 3 shows a model fit to one of the observations – radio source J1120+143 on 1995 September 8 – used in this paper. The cross-correlation function shows a skewed main peak with a kink at longer time lags indicating the definite presence of a second stream. Mauna Loa MkIII observations indicate that 10-20° at the tail-ends of the line of sight lay above the streamer belt and so is assumed to be in slow flow (Figure 2). The power law exponent α was set to 3.0, the inner scale to 35 km and the axial ratios of the fast and slow streams to 2.2 and 1.5 respectively. Model fitting gave the dominant fast stream a velocity of 883 km s^{-1} with a spread of 256 km s^{-1}. However, if the slow velocity were allowed to be fit, it was found to rise to approximately 700 km s^{-1} – fitting the kink in the cross-correlation function, but clearly well above the velocity expected for solar wind flow above the streamer belt. Hence, for this fit, it was fixed at 350 km s^{-1}, typical of slow wind speeds seen in IPS observations and by Ulysses.

A fit using the new model is given for the 1995 September 8 observation in Figure 4. The model used the same spectral parameters as before, but with two discrete fast streams and a second stream width in place of the uniform spread of velocities about the mean single fast stream. Faster and fast velocities of 875 km s^{-1} and 596 km s^{-1} respectively fitted best with a fast stream width of 16°. The model clearly fits the kink in the cross-correlation function. The quality of fit to the data using each model is best judged

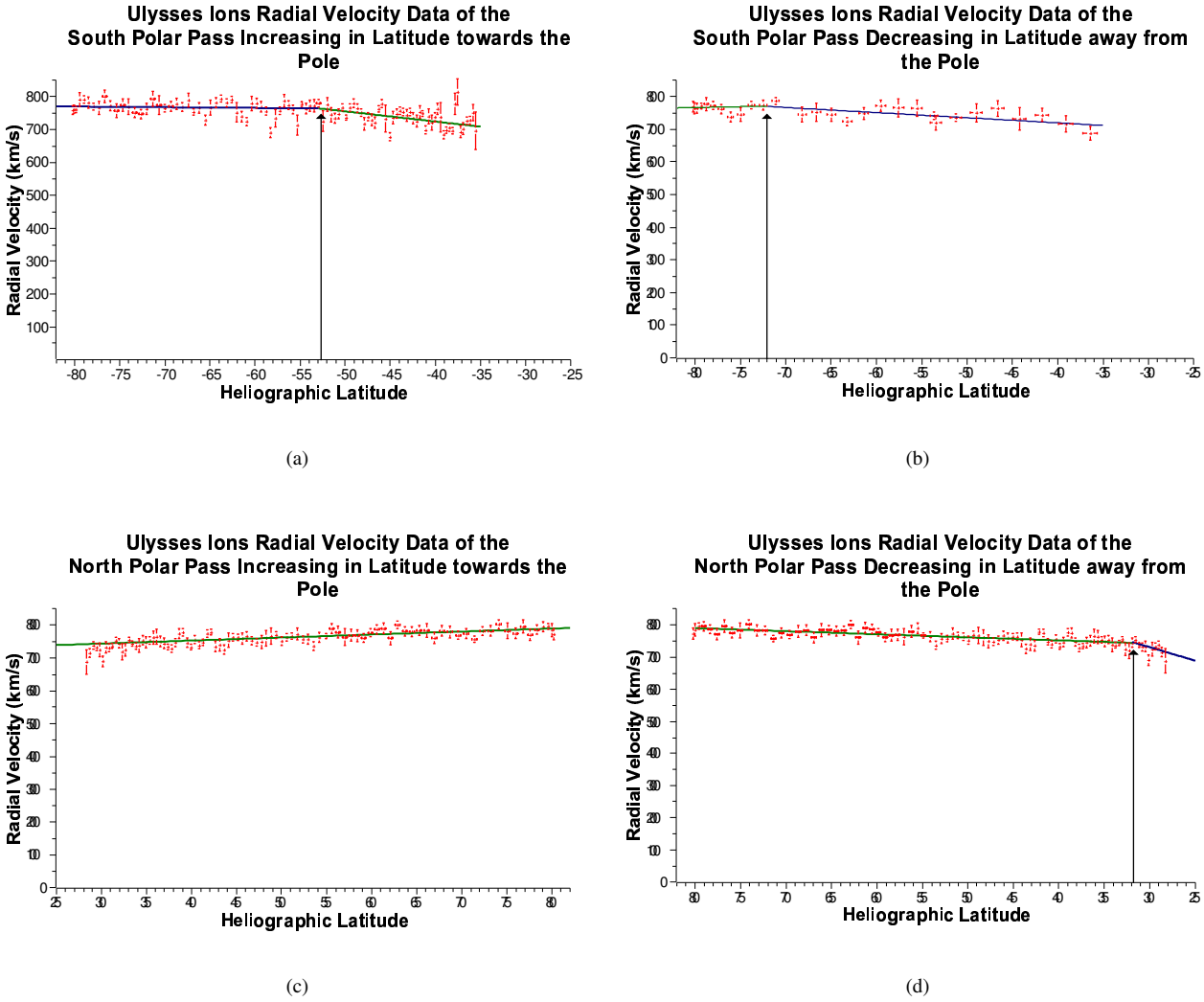

Figure 5. Plots of averaged Ulysses ions radial velocity for the first polar pass. The two lines represent the "best-fit" determined by the χ^2_ν fit to the binned data showing that a change in gradient of velocity with latitude fits the data best. The arrow indicates the inflexion point between the two lines. The latitude and χ^2_ν fit values can be seen in table 3.

by comparing the reduced-chi-square (χ^2_ν) parameter, as described in *Reiff* [1983], for the fits. In this example the original two-stream model (2 free parameters) gave $\chi^2_\nu = 1.88$ and the new three-stream model (3 free parameters) gave $\chi^2_\nu = 0.93$, indicating a significant improvement in the fit.

The IPS data presented in this paper are therefore analysed in the following way. Only the mean fast stream velocity and associated $\delta V_\parallel$ are fitted; all other parameters, including those of the slow stream, are chosen such that they best represent the data. The results of these fits were taken to represent the null-hypothesis result, in which the fast solar wind was best represented by a single stream with some finite variation in flow speed. Next, in order to determine whether the observations could be better represented using a two-mode fast wind, we used the three-stream model to fit two discrete fast velocities and a width in the line of sight for the second stream. All other parameters were left as in the two-stream fit. The quality of fit, as given by the χ^2_ν, combined with the values obtained in each fit are used to judge whether the observations are best described by two discrete fast streams. The width obtained for the second fast stream is then used to compare the boundaries of both fast streams with coronal hole boundaries seen in Yohkoh|SXT and SOHO|EIT synoptic maps. However, since this fit restricts the width of the second fast stream to be equal on each side of the line of sight, a further analysis is performed in which the width is set according to the EUV and X-ray coronal hole boundary and only the faster and fast stream velocities are fitted.

4. Results

Both EISCAT IPS observations and Ulysses|SWOOPS data were analysed as part of this investigation into the structure of the fast solar wind.

4.1. EISCAT IPS data

The main case results are summarised in table 1. Of the eight observations that met all of the criteria for a clear fast dominated flow, five of them (with χ^2_ν values highlighted in bold in the table) were clearly better fitted using the dual- fast wind model. The faster of the two streams was the stream at the higher latitude of the two streams. In all the remaining cases, neither of the model fits could be preferred over any other.

Only one case showed a best fit when the boundary between fast streams agreed with the coronal hole boundary seen in X-ray/EUV. In all the remaining cases, the model fitting indicated a boundary much lower in latitude than that seen in X-ray/EUV. However, these results do not indicate any strong or systematic relationship between the fast stream boundaries inferred from the IPS analyses

Table 2. Summary of Ulysses|SWOOPS ions analysis, the lowest χ^2_ν value closest to 1 are in bold.

Ulysses|SWOOPS Results				
Type/Order of fit	South increasing latitude	South decreasing latitude	North increasing latitude	North decreasing latitude
Straight-line	2.77866	1.00748	**0.48211**	1.13374
Two-stage gradient	**2.36277**	**1.00580**	0.46569	**1.06449**
X^2 parabola	2.42265	1.02292	0.47697	1.10716
X^3 parabola	2.39792	1.05332	0.49470	1.11038

Table 3. Summary of Ulysses|SWOOPS ions best-fit analysis

Ulysses|SWOOPS Results				
Variable	South increasing latitude	South decreasing latitude	North increasing latitude	North decreasing latitude
Latitude of change in gradient	(-52.95 +2.58/-1.50)°	(-72.48 +0.48/-0.93)°	Straight-line	(+31.94 +1.95/-1.04)°
Date of change in gradient	16/02/94: 1994, 46.60	30/10/94: 1994, 302.23	N/A	11/07/96: 1996, 192.48
Carrington rotation during change in gradient	1879	1888	N/A	1911
Days of year for the Carrington rotation	1994 - 37.96-65.29	1994 - 283.24-310.53	N/A	1996 - 180.70-207.90
Latitude of SXT coronal hole	60±10°	50±10°	50±10°	50±10°
Latitude of EIT coronal hole	Not available	Not available	Not available	60±10°
χ^2_ν of fit	2.362770	1.005800	0.482111	1.064490
Nu	94	26	27	89
Significance Level	$\ll 0.001$	~ 0.450	> 0.990	~ 0.300
Summary	No clear fit	Weak evidence for a bi-modal fast wind	Strong evidence for a single fast wind	Weak evidence for a bi-modal fast wind

and those obtained from EUV/X-ray Carrington maps. We therefore consider it important to compare these results with the one and only available set of high latitude in-situ solar wind data recorded, the SWOOPS measurements made by the Ulysses spacecraft while making its first polar pass at solar minimum.

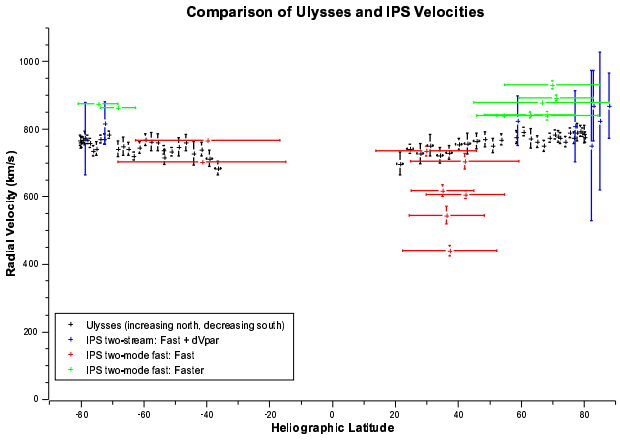

Figure 6. Figure showing the IPS fitted velocity values as a rough comparison to the values of the two most-significantly fitted Ulysses SWOOPS ions radial velocity binned data with latitude (south decreasing latitude and north increasing latitude). Two-stream modelled velocities (blue) are included simply as a measure of the range of velocities given by the IPS modelling, using half $\delta V_{\|}$ as the error; the latitude given is that of the point of closest approach. The 2-mode fast wind modelled fast (red) and faster (green) velocities used are from the best fit from each observation using errors quoted from the least-squares fitting routine; the latitude ranges given are derived from the average latitudes of the fast/faster wind boundaries and the fast/slow wind boundaries.

4.2. Ulysses SWOOPS in-situ data

The Ulysses SWOOPS ions hourly-averaged data were "binned" (averaged further) for approximately every 100 data points. In order to restrict the study to fast wind, a low-latitude cut-off point was established at the lowest latitude above which the solar wind velocity never dipped below 600 km s^{-1} in any of the original hourly averaged data points. The data were split into four different sections corresponding to the increasing and decreasing latitude parts of the northern and southern polar passes. Each section was then fitted with polynomials of orders 1 to 3 via a least-squares fitting method. A bimodal linear fit (i.e. straight line with a change in gradient) was also performed with the break-point between the two linear fits set to a range of latitudes from 75° N/S to 10° from the low-latitude cut-off.

Using the χ^2_ν value as a measure of the goodness of fit, the data appeared to be best represented by the bi-linear fit in three out of the four segments and a linear fit in one out of the four segments as shown in tables 2 and 3, and in figure 5. It should be noted that in those cases where a bi-linear fit gave the lowest χ^2_ν value closest to 1 in table 2, the improvement of fit gained was generally very small. It should also be noted that in the increasing latitude northern pole case, the χ^2_ν value is always over-fitted which is why the straight-line linear fit is taken as the most appropriate in this case. There was no clear relationship between the latitude of the inflection point of the bi-linear fits and the latitude of the coronal hole

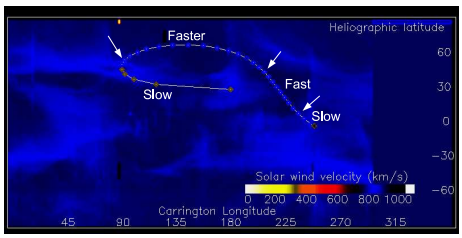

Figure 7. Synoptic map of LASCO east limb white light data from Carrington rotation 2016, overlayed by the IPS line of sight to 0319+415. The arrows indicate the positions of the fast/slow wind boundaries (as inferred from this image) and the fast/faster wind boundary as fitted using the 2-mode fast wind model.

boundary seen in X-ray or EUV emission during the same Carrington Rotation. The only clearly significant result indicated a single fast wind with higher velocities at higher latitudes, which is in good agreement with the results of *McComas et al.* [2000].

Figure 6 shows a rough comparison of the two-mode fast IPS best-fitted data and ion SWOOPS data, bearing in mind that the observations were taken at different times and so cannot be taken as a direct comparison. However, they can be used to get the general picture of the two different data-sets. To save overcrowding on the plot, only the most-significantly fitted Ulysses data from each hemisphere are used. The fast velocities and their associated spread ($\delta V_{\|}$) from the traditional two-stream model fits are used as an illustration of the range of velocities given by the IPS modelling. $\delta V_{\|}$ was not modelled in the 2-mode fast wind model fitting and so no spread in velocity can be inferred from these results. Instead they are used to illustrate the range of latitudes covered by each fast stream, as determined by the fast/slow wind boundaries and the fast/faster wind boundaries.

4.3. Extremely long baseline observation

Recent developments in the IPS observing technique have included the use of much more widely separated antennas with separations up to 2000 km in the radial baseline, carried out with EISCAT and the Multi-Element Radio Linked Interferometer Network (MERLIN) based in the United Kingdom (this experiment is described further in *Breen et al.* [2006]). The difference between time lags for solar wind speed increases as the antenna separation gets larger. An observation of 0319+415 from 2004 May 12 produced a correlation function that showed two clear fast wind peaks [*Bisi et al.*, 2005; *Breen et al.*, 2006].

This observation strongly suggested the presence of two distinct fast components which could be interpreted in two ways:

(i) As a region of faster flow from above the polar coronal hole at the crown and fast flow above the quiet Sun;

or

(ii) As faster flow from above the whole of the white light coronal hole and fast flow above the equator-ward boundary of the polar coronal hole.

The outflow from equator-ward boundaries of coronal holes is generally accepted to be slower than that from large polar holes [e.g. *Kojima et al.*, 2004]. Figure 7 shows the line of sight projected back along the Parker spiral (assuming radial outflow) and down to the solar corona at 2.5$R_{\odot}$ and overlaying a synoptic map of white light. The geometry of the observation does suggest that the Earthward side of the line of sight lies above an equator-ward boundary of the polar coronal hole. The transition between flow above a large polar hole and that above an equator-ward boundary would be fairly abrupt and lead to the appearance of two discrete fast components of flow.

To account for this scenario, a further modification was made to the analysis program to allow the width of the fast stream to be fitted on only one side of the line of sight. The IPS data were analysed using the 2-mode fast wind model (Figure 8) and the results are unambiguous: It is only possible to reproduce the shape of the cross-correlation function if the fast stream occupies part of the line of sight over the equator-ward boundary of the coronal hole. No other scenario would reproduce the correct shape. The stream boundaries in the IPS line of sight, as found in this analysis, are also marked in Figure 7.

This result provides convincing evidence of a greater degree of non-uniformity in the fast solar wind than is seen in the Ulysses|SWOOPS data.

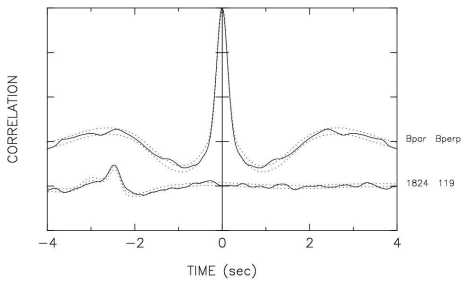

Figure 8. The EISCAT/MERLIN observation of 0319+415 on 2004 May 12, fitted with the 2-mode fast wind weak scattering model. Parameters are: V_{faster} 766 km s^{-1}; V_{fast} 640 km s^{-1}; axial ratio 2.0; θ_{in} -55°; θ_{out} 55°; V_{slow} 350 km s^{-1}; weighting 5.3; α 3.0; inner scale 85.0; fast stream width 40°(Earth end of the line of sight only). The χ^2_{ν} is 0.51.

5. Discussion

The results from IPS and in-situ measurements reported in this paper provide evidence for a change in character of the solar wind between the polar crown and the equator-ward flanks of the fast wind, but IPS results suggest a two-mode fast solar wind more strongly than do the in-situ data.

The polar fast wind is faster and appears to vary little with latitude whereas the wind above the lower latitude regions of the white light coronal hole shows a more marked decrease in velocity with decreasing latitude. These results are generally consistent with the Woo and Habbal proposals. However, the Ulysses results suggest a more continuous distribution of solar wind speeds rather than two distinct modes.

Although the majority of the IPS results indicate that a 2-mode fast wind model is a better fit to the measurements, the χ^2_{ν} values are high in many cases indicating that the model still does not adequately describe the data. A possible explanation for this is the steady variation in velocity with latitude of the flanking fast stream, as seen in the Ulysses data at lower latitudes, which has not been included in the 2-mode fast wind IPS model. The fact that some observations do not fit significantly better with the 2-mode fast wind model also suggests this explanation.

The boundary between fast and faster streams in the IPS lines of sight modelled in the IPS analysis showed no correlation with the coronal hole and quiet Sun boundary seen in EUV and X-ray measurements. This suggests that either there is no distinction between the fast wind emanating from the quiet Sun and the EUV/X-ray coronal hole, or that the individual fast wind components have interacted to a large enough extent for the boundary to be significantly blurred by IPS distances.

The extremely long baseline observation of 2004 May 12 does suggest two distinct modes of fast wind. However, in this case, the raypath extended from above the polar hole into a region above an equator-ward boundary of the northern hole. Analysis unambiguously indicated that the slower fast stream lay above the equator-ward boundary of the coronal hole. We therefore propose that the observation is dominated primarily by high-latitude, low density flow from across the raypath near the point of closest approach, and secondly, by slightly slower higher density flow above the equator-ward boundary of the coronal hole.

6. Conclusions

The results presented in this paper provide a useful test of the alternative models of fast wind internal structure. They reveal a difference in character between the flow found in interplanetary space above the polar crown and above the flanks of the white light coronal hole, though probably not a sudden transition from one type of flow to another.

Within the fast solar wind the latitudinal gradient in velocity in the polar crown stream is considerably shallower than that seen in the equator-ward flanks of the fast stream. However, the Ulysses data do not provide significant evidence of a bi-modal fast wind, though it could be the case that there is an inhomogeneity in the turbulence that damps out between IPS distances (typically ~50 $R_{\odot}$) and the typical distance of Ulysses (over 10 times that). It can

only suggest that there is a difference in character between the polar stream and the flanks of the fast wind.

We suggest that the flow observed above the centres of the polar coronal holes should be regarded as the archetypal fast wind. The change in latitudinal gradient in velocity observed in interplanetary space at latitudes near to those of the boundaries of the X-ray coronal holes may indicate an internal boundary within the fast wind or may simply be the signature of a more gradual change in solar wind properties. The presence of two distinct fast velocities in the EISCAT-MERLIN result strongly suggests a difference in character between the high-latitude fast wind found above the polar coronal hole, and the flow above the equator-ward boundary of the polar hole; it is also likely that this difference applies to flow above the centres of polar coronal holes and regions near their equator-ward boundaries.

Acknowledgments. We would like to thank the directors and staff of EISCAT and MERLIN for the IPS data used in this paper and for the supply of equipment whilst using these facilities. EISCAT is supported by the scientific research councils of Finland, France, Germany, Japan, Norway, Sweden and the United Kingdom. The MERLIN system is supported by PPARC, as were several of the authors of this paper (RAF, MMB, RAJ) during the time this work was carried out. The programs used to analyse the IPS data are based on routines developed by W.A. Coles and B.J. Rickett at the University of California, San Diego and we are extremely grateful not only for the programs but also for much valuable advice. SOHO|LASCO data are used courtesy of the LASCO consortium and were made available by the EIT consortium. We would also like to thank D.J. McComas and the Ulysses|SWOOPS team for the solar wind plasma data, A. Lecinski for the MkIII coronagraph white light data, and the Yohkoh consortium for the SXT data.

References

Acton, L. W., M. Bruner, W. Brown, J. Lemen, T. Hirayama, S. Tsuneta, T. Watanabe, and Y. Ogawara (1989), The Solar-A Soft X-Ray Telescope Experiment, *Advances in Space Research*, *8*(11), 93–99.

Armstrong, J. W., and W. A. Coles (1972a), Analysis of three-station interplanetary scintillation data, *Journal of Geophysical Research*, *77*, 4602–4610.

Bame, S. J., D. J. McComas, B. L. Barraclough, J. L. Phillips, K. J. Sofaly, J. C. Chavez, B. E. Goldstein, and R. K. Sakurai (1992), The Ulysses solar wind plasma experiment, *Astronomy and Astrophysics Suppliment*, *92*(2), 237.

Bisi, M. M., A. R. Breen, R. A. Fallows, P. Thomasson, R. A. Jones, and G. Wannberg (2005), Combined EISCAT/ESR/MERLIN Interplanetary Scintillation Observations of the Solar Wind, in *ESA SP-592: Solar Wind 11/SOHO 16, Connecting Sun and Heliosphere*, pp. 593–596, European Space Agency.

Breen, A. R., R. A. Fallows, M. M. Bisi, P. Thomasson, C. A. Jordan, G. Wannberg, and R. A. Jones (2006), Extremely long-baseline Interplanetary Scintillation measurements of Solar Wind velocity, *in press, Journal of Geophysical Research*.

Brueckner, G. E., R. A. Howard, M. J. Koomen, C. M. Korendyke, D. J. Michels, J. D. Moses, D. G. Socker, K. P. Dere, P. L. Lamy, A. Llebaria, M. V. Bout, R. Schwenn, G. M. Simnett, D. K. Bedford, and C. J. Eyles (1995), The Large Angle Spectroscopic Coronagraph (LASCO), *Solar Physics*, *162*, 357–402.

Canals, A. (2002), Interplanetary Scintillation Studies of the Solar Wind during the Rising Phase of the Solar Cycle, Ph.D. Thesis, The University of Wales, Aberystwyth.

Coles, W. A. (1996), A bimodal model of the solar wind speed, *Astrophysics and Space Science*, *243(1)*, 87–96.

Coles, W. A., R. R. Grall, T. Klinglesmith, and G. Bourgois (1995), Solar cycle changes in the level of compressive mircoturbulance near the sun, *Geophysical Research*, *100*.

Delaboudiniere, J. P., G. E. Artzner, J. Brunaud, A. Gabriel, J. F. Hochedez, F. Millier, X. Y. Song, B. Au, K. P. Dere, R. A. Howard, R. Kreplin, D. J. Michels, J. D. Moses, J. M. Defise, C. Jamar, P. Rochus, J. P. Chauvineau, J. P. Marioge, R. C. Catura, J. R. Lemen, L. Shing, R. A. Stern, J. B. Gurman, W. M. eupert, A. Maucherat, F. Clette, P. Cugnon, and E. L. van Dessel (1995), EIT: Extreme-Ultraviolet Imaging Telescope for the SOHO Mission, *Solar Physics*, *162*, 291–312.

Dennison, P. A., and A. Hewish (1967), The solar wind outside the plane of the ecliptic, *Nature*, *213*, 343–346.

Dupree, A. K., M. J. Penn, and H. P. Jones (1996), He i 10830 Angstrom Wing Asymmetry in Polar Coronal Holes: Evidence for Radial Outflows, *Astrophysical Journal*, *467*, L121+.

Fallows, R. A., P. J. S. Williams, and A. R. Breen (2002b), EISCAT measurements of solar wind velocity and the associated level of interplanetary scintillation, *Annales Geophysicae*, *20*, 1279–1289.

Fisher, R. R., R. H. Lee, R. M. MacQueen, and A. I. Poland (1981), New Mauna Loa Coronagraph Systems, *Appl. Op.*, *20*, 1094–1101.

Goldstein, B. E., M. Neugebauer, J. L. Phillips, S. Bame, J. T. Gosling, D. McComas, Y.-M. Wang, N. R. Sheeley, and S. T. Suess (1996), ULYSSES plasma parameters: latitudinal, radial, and temporal variations., *Astronomy and Astrophysics*, *316*, 296–303.

Habbal, S. R., and R. Woo (2001), Connecting the Sun and the Solar Wind: Comparison of the latitudinal profiles of coronal and Ulysses measurements of the fast wind, *The Astrophysical Journal*, *549*(2), L253–L256.

Hassler, D. M., I. E. Dammasch, P. Lemaire, P. Brekke, W. Curdt, H. E. Mason, J. C. Vial, and K. Wilhelm (1999), Solar wind outflow and the chromospheric magnetic network, *Science*, *283*, 810–+.

Klinglesmith, M. (1997), The Polar Solar Wind from 2.5 to 40 Solar Radii: Results of Intensity Scintillation Measurements, Ph.D. Thesis, University of California, San Diego (UCSD).

Kojima, M., A. R. Breen, K. Fujiki, K. Hayashi, T. Ohmi, and M. Tokumaru (2004), Fast solar wind after the rapid acceleration, *Journal of Geophysical Research (Space Physics)*, *109*(A18), 4103.

Little, L. T., and R. D. Ekers (1971), A method for analysing drifting random patterns in astronomy and geophysics, *Astronomy and Astrophysics*, *10*, 306–309.

McComas, D. J., B. L. Barraclough, H. O. Funsten, J. T. Gosling, E. Santiago-Munoz, R. M. Skoug, B. E. Goldstein, M. Neugebauer, P. Riley, and A. Balogh (2000), Solar wind observations over Ulysses' first polar orbit, *Journal of Geophysical Research*, *105*(A5), 10,419–10,433.

Ogawara, Y. (1987), The SOLAR-A Mission, *Solar Physics*, *113*, 361–370.

Ogawara, Y., T. Takano, T. Kato, T. Kosugi, S. Tsunta, T. Watanabe, I. Kondo, and Y. Uchida (1991), The Solar-A Mission: An Overview, *Solar Physics*, *136*, 1–16, kluwer Academic Publishers - Printed in Belgium.

Phillips, J. L., S. J. Bame, W. C. Feldman, B. E. Goldstein, J. T. Gosling, C. M. Hammond, D. J. McComas, M. Neugebauer, E. E. Scime, and S. T. Suess (1995), ULYSSES Solar Wind Plasma Observations at High Southerly Latitudes, *Science*, *268*, 1030–+.

Reiff, P. H. (1983), The use and misuse of statistical analyses, in *ASSL Vol 104: Solar-Terrestrial Physics: Principles and Theoretical Foundations*, p. 493.

Rishbeth, H., and P. J. S. Williams (1985), Ionospheric Radar: the system and its early results, *Monthly Notices of the Royal Astronomical Society*, *26*, 478–512.

Wannberg, G., L.-G. Vanhainen, A. Westman, A. R. Breen, and P. J. S. Williams (2002), The new 1420 MHz dual polarisation interplanetary scintillation (IPS) facility at EISCAT, in *Conference Proceedings*, Union of Radio Scientists (URSI).

Woch, J., W. I. Axford, U. Mall, B. Wilken, S. Livi, J. Geiss, G. Gloeckler, and R. J. Forsyth (1997), SWICS/ULYSSES Observations: The Three-Dimensional Structure of the Heliosphere during Solar Minimum, in *Solar Wind Papers*, Max-Planck-Institut Für Aeronomie.

Woo, R., and S. R. Habbal (1997), Extension of coronal structure into interplanetary space, *Geophysical Research Letters*, *24*(10), 1159–1162.

Yamauchi, Y., M. Kojima, M. Tokumaru, H. Misawa, H. Mori, T. Tanaka, H. Takaba, T. Kondo, and P. K. Manoharan (1996), Micro-turbulence in the solar wind at 5-76 rs observed with interplanetary scintillation, *Journal of Geomagnetism and Geoelectricity*, *48*, 1201–1217.

M. M. Bisi, Center for Astrophysics and Space Sciences, University of California, San Diego, 9500 Gilman Dr., La Jolla, CA 92093 (mmbisi@ucsd.edu or Mario.Bisi@gmail.com)